Surface freezing in chain molecules. II. Neat and hydrated alcohols

O. Gang,[1] X. Z. Wu,[2,*] B. M. Ocko,[3] E. B. Sirota,[4] and M. Deutsch[1]
[1]*Physics Department, Bar Ilan University, Ramat Gan 52900, Israel*
[2]*Physics Department, Northern Illinois University, DeKalb, Illinois 60115*
and Material Sciences Division, Argonne National Laboratory, Argonne, Illinois 60439
[3]*Physics Deparment, Brookhaven National Laboratory, Upton, New York 11973*
[4]*Exxon Research and Engineering Company, Route 22 East, Annandale, New Jersey 08801*
(Received 1 April 1998)

Surface freezing is studied in dry and hydrated normal-alcohol melts by x-ray scattering and surface tensiometry. A single crystalline bilayer forms at the surface, for even carbon numbers only, at temperatures up to 1 °C (dry) or 2 °C (wet) above the bulk freezing, and persists without change down to bulk freezing. The packing is hexagonal, with untilted molecules for short chains and tilted molecules for long chains. The lattices of the upper and lower monolayers are shifted along the next-nearest-neighbor direction. Hydration is found to swell the bilayer by ~ 2.5 Å due to water intercalation into the bilayer, at a molecular water:alcohol ratio of $\sim 1{:}2$. It also increases the transition temperatures, and the temperature and chain-length ranges for which surface crystallization is observed. These effects are accounted for quantitatively by considering the surprising *increase* in hydration upon freezing, and taking into account the Gibbs-rule-predicted water depletion at the surface in the liquid surface phase. [S1063-651X(98)15010-9]

PACS number(s): 68.10.−m, 61.25.Em, 64.70.Dv

I. INTRODUCTION

Surface freezing, the formation of a crystalline layer at the surface of a one-component melt at a temperature higher than its bulk freezing point, was originally observed in normal-alkanes [1–3]. The *n*-alkane molecule is a methyl-terminated linear hydrocarbon chain, having a full molecular inversion symmetry with respect to its center, and is well represented by a cylindrical envelope in its rotator phase [4]. The molecule is nonpolar, and interacts solely by van der Waals (vdW) forces [5]. The surface-frozen layer is found to be a single molecule thick, crystalline with hexagonal packing, and exists for a temperature range of $\Delta T \leqslant 3$ °C above the bulk freezing temperature for chain lengths $16 \leqslant n \leqslant 50$. The properties and structure of the surface-frozen monolayer in *n* alkanes are described in detail in Ref. [6] (hereafter denoted I), and references therein. While considerable progress has been made toward a theoretical understanding of the origins of this effect [7–11], many basic issues still remain open. One key question is how are these properties, and indeed the very existence of the surface freezing effect, influenced by deviations from the simple molecular structure and/or simple intermolecular vdW interactions of the alkanes? To explore these issues we have chosen to study normal 1-alcohols, $CH_3(CH_2)_{n-1}OH$, denoted here C_nOH. This molecule is almost identical with *n*-alkanes, the only difference being the exchange of an H on one terminal methyl by a hydroxyl OH group. This small structural deviation breaks the inversion symmetry and renders the molecule slightly polar. Moreover, it modifies the molecular interactions, since it allows for the formation of hydrogen bonds (HB's) between adjacent molecules through their hydroxyl groups. Finally, very recent studies of water-supported Langmuir monolayers of *chiral* 2-alcohols (having their OH groups on the second carbon of the chain) have shown marked structural and stability deviations from those of the *nonchiral* 1-alcohols [12]. Thus, measurements on 1-alcohols should provide a base line against which 2-alcohols, and other chiral molecules like 1,2-diols (linear hydrocarbon chain with hydroxyl groups on the first and second carbons) can be compared to elucidate the effects of chirality on surface freezing.

Using synchrotron x-ray surface scattering and surface tension techniques we have studied surface freezing in 1-alcohols. We find that surface freezing exists in alcohols as well, although the surface layer is now a bilayer rather than a monolayer. Also, the effect is observed only in molecules with an even number of carbons, unlike alkanes, where it occurs for both odd and even n. The hydroxyl groups of the upper and lower layers point to the center of the bilayer, allowing its stabilization by HB's between the OH groups. The structure of the bilayer is determined both normal to the surface and in-plane over the full chain-length–temperature phase diagram. We find two two-dimensional rotator phases, one with vertically aligned molecules, and the other with molecules tilted towards next-nearest neighbors at an *n*-dependent angle. For the hydrated alcohols an *n*-independent swelling of the surface bilayer was observed, resulting from the intercalation of water into the center of the bilayer, at an approximate ratio of one water molecule per two alcohols. Hydration also changes the chain-length–temperature phase diagram in a way which indicates that, for $n \sim 12$, the hydrogen bonding has a major influence on the structure and on the occurrence of surface freezing, while for $n \sim 30$ its influence is negligible.

In the following sections we deal with the experimental techniques and the data fitting procedures, discuss the results obtained from the measurements and the fits for both dry and hydrated alcohols, and point to the implications of these re-

*Present address: IBM Almaden Research Center, 650 Harry Rd., San Jose, CA 95120-6099.

sults for the basic mechanism underlying surface freezing in alcohols and the interplay between the various interactions taking part in the determination of the bilayer's structure.

II. EXPERIMENT

The structure of the surface was explored by x-ray techniques, and the thermodynamics by surface tension measurements. Since the experimental methods were described in detail in I, only feature peculiar to the alcohol measurements will be discussed here.

A. Samples and cell

The experimental cells used in the surface tension and x-ray scattering measurements are the same as those used in I. The alcohols were obtained from Sigma, Fluka or Aldrich with a nominal 99% purity or higher, and used as received. Samples were prepared by spreading $\lesssim 1$ g of melted material on a 2-in.-diameter thin copper plate, placed in the temperature regulated ($\lesssim 0.005\,^{\circ}\mathrm{C}$) cell. In the hydrated alcohol experiments a ring shaped container with 2–3 cm^3 of water surrounded the plate, generating a saturated water vapor atmosphere in the cell. The sample was thus hydrated by absorbing water from the vapor phase. Identical results were obtained in a few tests for samples hydrated by contact with water drops, or direct mixing with water. When the water was allowed to evaporate from the cell after the completion of the measurements, the measurements reproduced exactly the results obtained in the initial, dry-sample experiments for both the surface tension and x-ray measurements.

B. X-ray measurements

The x-ray measurements were carried out at the Harvard/BNL liquid surface diffractometer on beamline X22B, National Synchrotron Light Source, Brookhaven National Laboratory, with a typical wavelength of $\lambda = 1.54$ Å. The density profile of the vapor-liquid interface was studied by x-ray reflectivity (XR) and the in-plane structure by grazing incidence diffraction (GID) and Bragg rod (BR) measurements. The bilayer structure mandated the use of a somewhat different BR analysis than that presented in I, since now an interference from rays originating in the lower and in the upper layers, as well as a possible shift between the lattices in those two layers, had to be accounted for. The expressions employed are discussed below.

C. Surface tension measurements

Surface tension measurements were used to probe the thermodynamics of surface freezing. The Wilhelmi plate method [13] was employed, with plates cut from filter paper, to enhance wetting by the alcohol melt. A disadvantage of this necessity is that it requires changing the paper plate from sample to sample to avoid contaminations. Thus unavoidable differences in the cutting of the paper to size increased the scatter of the data points by $\sim 5\%$ relative to that obtained when using the same plate throughout. The plate is attached to an electronic balance, which measured the tension. The samples were contained in a temperature regulated cell, which is basically the same as the one used for the x-ray measurements, except that it has a small hole in its cover to pass the wire connecting the balance to the plate. Each data point is an average of 20 measurements at a fixed temperature, taken within a period of 30 s. The temperature was varied stepwise at a rate $\leqslant 0.3\ \mathrm{m\,^{\circ}C\,s^{-1}}$ to ensure ample thermal equilibration. Slower scan rates, and changing the scan direction, did not alter the results. The whole setup was computer controlled.

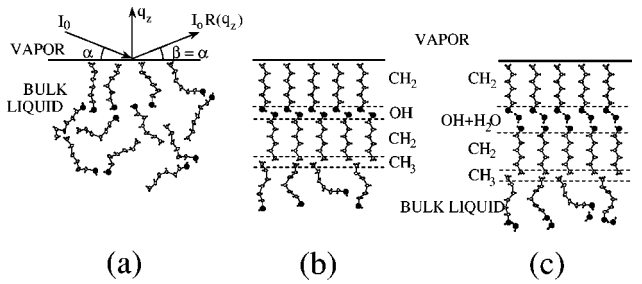

FIG. 1. Schematic molecular arrangement at the surface of an alcohol melt in its high-temperature liquid state (a), and in the surface-frozen phase, with the bulk remaining liquid, when (b) dry and (c) hydrated. The geometry of x-ray reflectivity at the vapor-liquid interface is given in (a). As the incidence and detection angles are equal ($\alpha = \beta$) the momentum transfer q_z is normal to the surface.

III. RESULTS AND DISCUSSION

The molecular order at the surface in the liquid, and in both the dry and hydrated surface-frozen phases, as derived from the x-ray measurements, are shown schematically in Fig. 1. Some of the dry alcohol results were discussed previously [14], and will, therefore, be addressed here only briefly. All other results, and in particular those of the hydrated alcohols, are discussed in detail in the following sections.

A. Dry alcohol melt

1. Surface-normal structure

The surface-normal structure was explored by XR measurements. Figure 2 shows the XR curve $R(q_z)$ [$q_z = (4\pi/\lambda)\sin\alpha$, where α is the incidence angle relative to the surface] measured for three different alcohol at two temperatures each: one above (triangles) and one below (circles) the surface freezing temperature T_s. At the higher temperature, $R(q_z)$ decreases monotonically with q_z, as typical for liquid surfaces. It is well described by $R(q_z) = R_F(q_z)\exp(-q_z^2\sigma^2)$, where $R_F(q_z)$ is the Fresnel reflectivity for an ideally flat and smooth interface, and the factor $\exp(-q_z^2\sigma^2)$ arises from a Gaussian distributed interfacial roughness with an effective height σ [6,15]. This roughness is mainly due to thermally excited capillary waves [16]. Just above T_s, the reflectivities can be fitted well (solid lines) with $\sigma = 4.5 \pm 0.1$ Å and a bulk electron density $\rho_\infty = 0.279$ $e/\mathrm{Å}^3$ for samples of all carbon numbers, n, as seen in Fig. 2. The corresponding electron density is given in a dash line in the inset. Below T_s, modulations suddenly appear in the reflectivities, indicating the appearance of a surface layer of a density different from that of the bulk. The interference be-

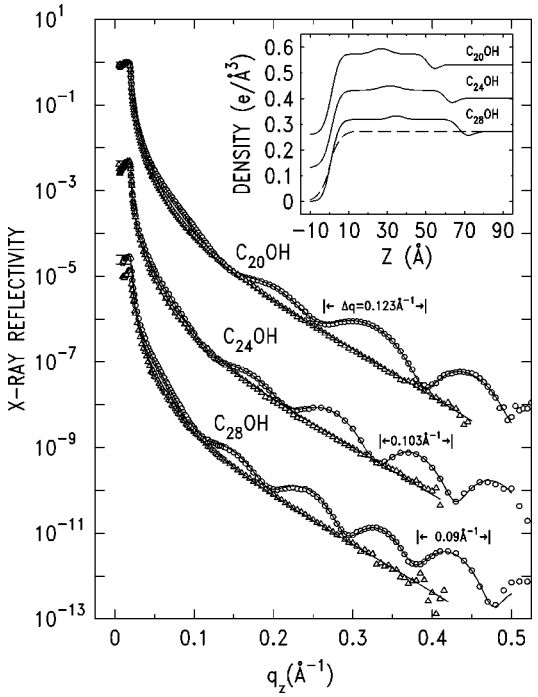

FIG. 2. X-ray reflectivities of neat liquid alcohols with $n=20$, 24, and 28 in their liquid surface phase (open triangles) and in the surface crystalline bilayer phase (open circles). The modulation periods Δq, discussed in the text, are marked on the figure. The solid lines are fits using the model density profile for the surface crystalline bilayer discussed in the text. The density profiles corresponding to the fits, for the crystalline (——) and liquid ($- - -$) surface phases are shown in the inset.

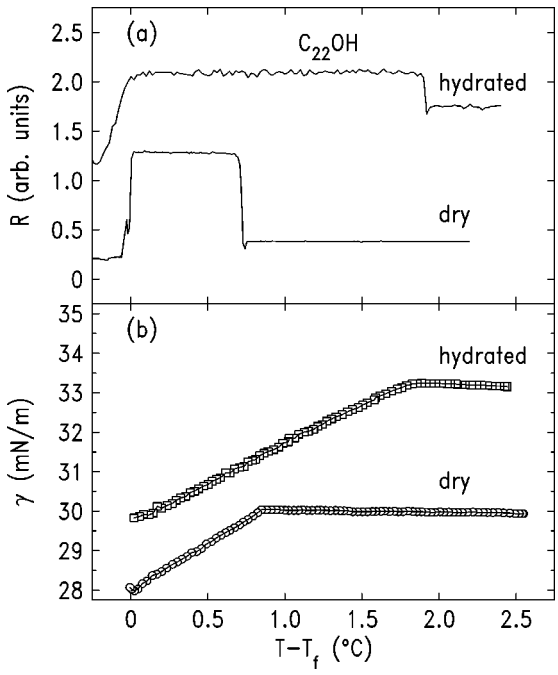

FIG. 3. (a) X-ray reflectivity R of $C_{22}OH$ at a fixed $q_z=0.2$ Å^{-1} in the dry and hydrated states. The intensity increases upon the surface layer formation, at T_s, and drops abruptly upon bulk solidification at T_f. (b) Surface tension of $C_{22}OH$ upon cooling from the high-temperature liquid surface phase, for a dry and hydrated sample. The surface freezing transition is marked by the sudden change of the slope from negative to positive. Note the much-increased temperature range of existence of the surface crystalline phase when hydrated.

tween rays reflected from the lower and upper interfaces of this layer leads to a $\cos(q_zD)$ modulation of the intensity, where D is the layer thickness. Using the measured modulation periods (marked on the figure) $\Delta q_z \approx 0.123$, 0.103, and 0.090 Å^{-1}, for $n=20$, 24, and 28, we estimate $D \approx 51$, 61, and 70 Å, respectively. These lengths are roughly *twice* the corresponding fully extended molecular lengths, indicating that a bilayer is formed at the surface. For *n*-alkanes, by contrast, the surface crystalline phase consists of a single molecular layer [2,3,6], which is reflected in the corresponding modulation periods being twice as long (see Fig. 4 in I). The present surface bilayer structure is very similar to the structure observed for the bulk rotator phase immediately below T_f, the bulk freezing temperature [17,18].

X-ray reflectivity can be used also to follow the formation of the surface layer, and detect variations in its structure with temperature. Figure 3(a) presents a so-called ''T scan,'' where the spectrometer is positioned at a fixed incidence angle at which the reflectivities of the liquid and frozen surface phases differ greatly (e.g., $q_z=0.2$ Å^{-1} for dry $C_{22}OH$, shown in the figure), and the intensity variation is recorded upon lowering of the temperature from above T_s to below T_f. As seen in the figure, the formation of the surface bilayer is observed as a sharp jump in the reflectivity. Within our accuracy of a few m °C, the transition is discontinuous, i.e., first order, as expected of a freezing transition, and as found in I for surface freezing in alkanes. The constant reflectivity for $T_f \leqslant T \leqslant T_s$ indicates that no further structural changes occur until bulk freezing is reached. In particular, no additional monolayers or bilayers are formed, showing the formation of the surface phase, when considered as a wetting effect, to follow a strongly incomplete wetting scenario [19]. The disappearance of the reflected signal at T_f is due to the macroscopic roughening of the surface upon the bulk crystallization.

The reflectivity curves in the surface crystalline phase were analyzed quantitatively using a layered interface model [6]. This model consists of four slabs [see the schematic model in Fig. 1(b)]: two slabs of equal electron density corresponding to the upper and lower layers of CH_2 chains, one slab of extra electron density at the center of the bilayer, corresponding to the denser OH headgroups, and one slab for the less-dense CH_3 depletion layer at the bilayer-liquid interface. The CH_3 depletion layer at the bilayer-vapor interface is absorbed into the surface roughness of that interface, and does not require a representation by an individual slab. All slabs were found necessary to obtain a good fit. The density profiles obtained from the fit, are shown in the inset of Fig. 2, along with that of the liquid surface of $C_{28}OH$ (dash line). For all the alcohols, the average electron density obtained for the surface bilayer, i.e., the slab corresponding to the CH_2 chains, was $\rho_s=0.309\pm0.009$ e/Å^3, about 10% higher than the average bulk liquid density 0.279 e/Å^3. The surface density is close to the bulk rotator phase density of 0.300 e/Å^3 [5], but slightly lower than the surface density of surface-frozen *n*-alkane monolayers, 0.317 ± 0.005 e/Å^3 [2,6].

The experimental conditions do not allow for a resolution of both the thickness and electron density of the depletion

and the enhancement slabs, which are both thin, and their density deviates only little from that of the CH_2 slab. The only refinable parameter for these two slabs is their integrated contribution to the density profile, $\delta\rho\,\delta d$, where $\delta\rho$ is the electron density excess (or depletion) relative to ρ_s and δd is the thickness of the layer. The fit yields $\delta\rho\,\delta d = 0.22 \pm 0.03$ and -0.27 ± 0.03 $e/\text{Å}^2$, for the OH and CH_3 slabs, respectively. The CH_3 slab value overlaps, within the combined experimental errors, with the $\delta\rho\,\delta d = -0.33 \pm 0.03$ $e/\text{Å}^2$ value found for alkanes [6]. Since the cross section area A of each molecular chain is constant at ~ 20 Å^2 (see below), the CH_3 group must have an actual length s larger than the nominal 1.27 Å of a single CH_2 unit [6] to create a depletion zone. With a monolayer–bulk average density $\rho = 0.293$ $e/\text{Å}^3$, and the nine electrons of the CH_3 group, s is related to $\delta\rho\,\delta d$ by $[9/(sA) - 0.293]s = \delta\rho\,\delta d = -0.27$ $e/\text{Å}^2$. This yields, for the depletion layer thickness, $s = 2.5 \pm 0.1$ Å, consistent with bulk alcohol crystals [17] and the 2.7 ± 0.2 Å obtained for the n-alkane surface crystals [6]. We can similarly calculate the thickness of the slab at the center of the bilayer, which contains two OH headgroups within the ~ 20 Å^2 cross-sectional area of the molecule. For the $2 \times 9 = 18$ electrons of the two OH groups and $(18/tA - 0.293)t = 0.22$ $e/\text{Å}^2$, we obtain for the enhancement slab a thickness of $t = 2.3 \pm 0.1$ Å, about 10% less than the nominal 2×1.27 Å of two CH_2 groups.

In Fig. 4(a) we plot *half* the dry bilayer thicknesses $d = D/2$ (listed in Table I) for the measured range of molecular lengths (circles). Also plotted is the calculated fully extended lengths of the molecules (line), $d_{\text{calc}} = 1.27 \times (n-1) + 2$ Å, where 1.27 Å is the projected length of the C-C bond along the chain, and the extra 2 Å accounts approximately for the size of the end group [5]. For $n \leqslant 22$, d agrees well with d_{calc}, implying that the alcohol chains in the bilayer are fully extended and aligned normal to the surface. For $n > 22$, we obtain $d < d_{\text{calc}}$, indicating that the chains in the bilayer are either tilted or not fully extended.

The four-layered interface model above includes, in principle, a roughness parameter for each of the five interfaces. As the present model has already a large number of parameters because of the bilayer structure and the three types of molecular groups (CH_3, CH_2, and OH), not all parameters could be determined simultaneously with confidence if a different roughness was allowed for each interface. Testing several combinations, it was found that three independent roughness parameters were sufficient, for (1) the bilayer-vapor interface (2) both interfaces of the OH layer, and (3) both interfaces of the lower CH_3 layer. Of these, the last two were basically independent of n. The first, σ_1, at the bilayer-vapor interface, varied with n. The resultant fits are those shown in Fig. 2, and the corresponding $D/2$ values are listed in Table I. The uncertainty in σ_1 was found to be about ± 0.4 Å. This uncertainty, though not large, is about the same as the n variation of σ_1 predicted by capillary wave theory (CWT) for the relevant temperature range. It prohibits, therefore, the extraction of the n-dependence of σ_1, and of the determination of any possible deviations from CWT, as found in I for alkanes [8]. To better assess the n variation of σ_1 we have carried out another set of fits assuming an identical roughness $\sigma_1 = \sigma_2 = \sigma_3 \equiv \sigma$ for all interfaces of the

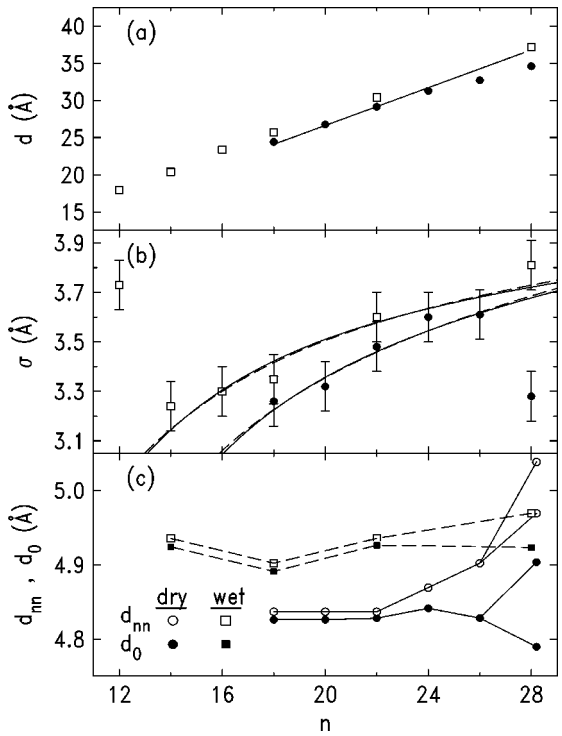

FIG. 4. As a function of the carbon number n, (a) the half-thickness $d = D/2$ of the bilayer, as obtained from the fit to the reflectivity curves for dry (circles) and wet (squares) alcohols, along with the estimated fully extended chain length (line). (b) The liquid-vapor interface roughness obtained from the fit. The lines are fits to a linear T (solid) and $T^{1/2}$ (dash) dependences, discussed in the text. Note the sharp decrease in the roughness for the dry $C_{28}OH$, which may indicate a crystalline, rather than a rotator, surface phase for the dry, but not for the hydrated, alcohol. (c) The chain-chain spacing in the surface plane (d_{nn}, open symbols) and in the plane normal to the molecular axis (d_0, closed symbols) derived from the grazing incidence diffraction measurements. The lines are just guides to the eye.

model, including the bilayer-vapor one. Although the χ^2 of the fit deteriorated, in a few cases by as much as a factor of 2–3 as compared to the best separate-roughness fits, the overall agreement with the measured data and, in particular, with the other parameter values refined in the separate-roughness fits, remained good. The σ values thus obtained had considerably smaller uncertainties (± 0.1 Å), and are plotted in Fig. 4(b). Note the monotonic increase with n for $n \leqslant 26$. As shown in the figure, the increase is consistent with the $\sqrt{T}$ behavior (dashed line) predicted by CWT, although the short range of the molecular lengths and the concomitant temperature range, do not allow the exclusion of a linear T dependence (solid line). This T dependence was found to prevail in alkanes, and was shown by Tkachenko and Rabin [8,7] to support their theory of entropy-stabilized surface freezing in chain molecules.

An intriguing feature in Fig. 4(b) is the drop of σ for $C_{28}OH$ by about 10% from that of $C_{26}OH$, in contrast with the monotonically increasing trend with n. A similar effect, with a comparable relative drop in σ, was found for alkanes at C_{44}, and was shown in I to result from the appearance of a new surface phase, where the molecules' rotational degrees of freedom freeze out, and a crystalline, rather than a rotator,

TABLE I. Experimental results of the x-ray and surface tension measurements for dry alcohol melts. n is the carbon number, $D/2$ the XR-measured half of the bilayer thickness, and $q_{\|}, q_z$ the in-plane GID and BR peak positions. The bulk freezing temperature T_f and the temperature range of existence ΔT of the surface crystalline phase were derived from the x-ray and surface tension measurements independently. θ is the molecular tilt angle from the vertical, derived from the BR measurements. The entropy change upon surface freezing, ΔS_s, is calculated from the difference in slope of the surface tension below and above the layer formation temperature, T_s. The corresponding bulk value ΔS_b was obtained from published values [17].

n	$D/2$ (Å)	$q_{\|}$ (Å^{-1})	q_z (Å^{-1})	θ (°)	T_f (°C)	ΔT °C)	ΔS_s (mJ m^{-2} K^{-1})	ΔS_b
12					21.1			
14					37.0			1.33
16				<5.0	49.0	0.15	1.4	1.66
18	24.42	1.50	0.1	<5.0	57.15	0.6	1.7	1.82
20	26.75	1.50	0.1	<5.0	63.7	0.8	1.75	2.18
22	29.15	1.50	0.09	<5.0	69.8	0.9	2.3	2.40
24	31.29	1.49	0.16	12.0	73.95	0.8	2.4	2.70
26	32.71	1.48	0.26	22.0	77.4	0.65	2.75	2.96
28	34.61	1.46	0.24	17.0	81.2	0.9	2.6	
		1.44	0.47					
30					84.0			

surface phase results. We discuss below the possibility of the occurrence of a similar rotator-to-crystal phase transition here. If indeed this is the case here, the decrease in σ is likely due to the decrease in the large translational disorder along the molecules' axis, characteristic of the rotator phase [20]. Alternatively (or even in parallel), the decrease in σ may indicate an increase in the bending rigidity K of the bilayer, from a near-zero value to a finite value, accompanying the transition from a plastic-crystalline (rotator) to a crystalline phase.

2. Surface-parallel structure

a. Grazing incidence diffraction. To probe the structure within the surface plane, grazing incidence diffraction measurements were carried out. The in-plane resolution of these measurements, $\Delta q_{\|} = 7 \times 10^{-3}$ Å^{-1}, was achieved by using Soller slits. For all n, a single in-plane peak was observed at $q_{\|} \sim 1.50 \pm 0.01$ Å^{-1} (except for $C_{28}OH$, described below, where two in-plane peaks were observed), indicating a hexagonal packing within the surface plane. The peak position remains constant for $n \leqslant 22$, and gradually decreases with n for $n \geqslant 24$, indicating an increase in the lattice spacing. The nearest-neighbor chain separations *in the surface plane* is given by $d_{\mathrm{nn}} = 2\pi/(q_{\|} \cos 30°)$ for our case of hexagonal packing. Using the q_z positions of the in-plane peaks (Table I), obtained from the Bragg rod measurements below, the scattering vector at the peak is given by $q = \sqrt{q_{\|}^2 + q_z^2}$, and hence the nearest-neighbor spacing *viewed along the chain axis* is given by $d_0 = 2\pi/(q \cos 30°)$. Both d_{nn} and d_0 are plotted in Fig. 4(c). An increase in d_{nn} for $n \geqslant 24$ is clearly observed, while d_0 remains constant for all n. These results, along with the layer thickness variation discussed above,

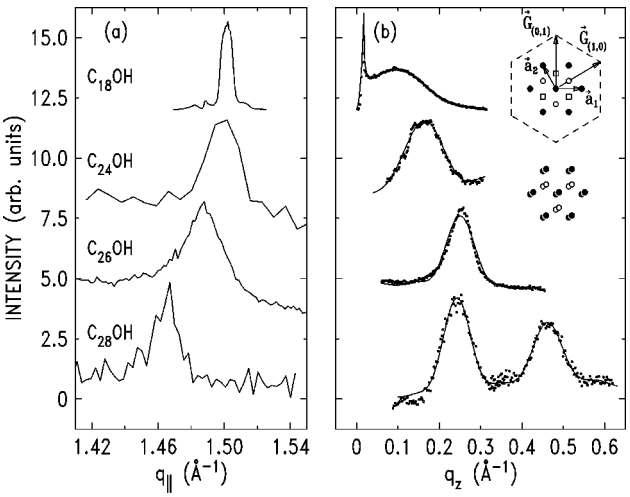

FIG. 5. The in-plane diffraction peaks for the dry alcohols (a), and the corresponding Bragg rods (b). The solid lines in (b) are the fits, for a hexagonal packing and the layer stacking discussed in the text and shown schematically in the insets to (b). The rod of $C_{18}OH$ is typical of vertically aligned molecules, while all others indicate a tilt toward next-nearest neighbors. Note that for $C_{28}OH$ two peaks are observable in the rod. Also, a second in-plane peak is observed, only for this compound, corresponding to the higher-q_z peak in the Bragg rod. These observations support the identification of the bilayer as crystalline for $C_{28}OH$.

clearly shows that for $n \geqslant 24$ the molecules tilt away from the normal. They do so rigidly, with the axis-normal distance of adjacent molecules remaining constant. These conclusions are also supported by the Bragg rod measurements discussed below.

The area occupied by one chain is 20.3 Å^2, based on the chain-chain spacing of 4.84 Å. The resultant electron density of the alkyl chain, having eight electrons per CH_2 group and a projected length of 1.27 Å along the molecular axis, can be then estimated directly as $8/(20.3 \times 1.27) = 0.310$ e/Å^3, in excellent agreement with the value 0.309 e/Å^3 obtained in the XR measurements. Since the reflectivity measurements probe the macroscopic x-ray-illuminated area, averaging over both crystalline and (possible) disordered regions, while the GID probes the crystalline part only, this agreement is a strong indication of a complete coverage of the surface by the crystalline bilayer. The area per alcohol molecules is about 3% larger than the 19.7 Å^2 found per alkane molecule of the same length, presumably due to the bulkier headgroup. This is also consistent with the fact that the electron density of the alcohol layer, 0.309 e/Å^3, obtained above from the XR, is 97.5% of the 0.317 e/Å^3 measured for alkanes in I.

Figure 5(a) shows the in-plane peaks for several n, where the $q_{||}$ peak position decreases (as discussed above), and width increases with n for $n \geqslant 24$. For $n \leqslant 22$, the in-plane peak is resolution limited, indicating that the coherence lengths are at least several thousand Å. Measurements of the peak intensity *vs* azimuthal rotation of the sample show that the sample surface is covered by only a few very large crystals. Coverage considerations [21] indicate that these are of at least a few millimeters in size. For $n \geqslant 24$, an azimuthal sample rotation at the GID peak position results in an almost constant intensity. This indicates that for these n the surface is covered with many small crystals, i.e., the surface bilayer

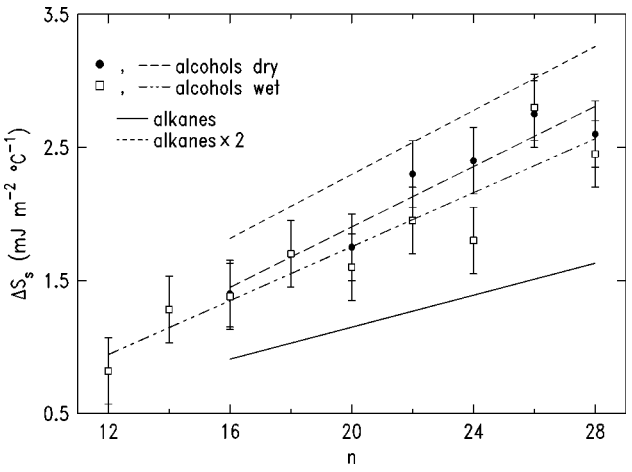

FIG. 6. The slope differences as derived from the surface tension measurements for the dry (circles) and hydrated (squares) alcohols, along with straight lines fitted to them as guides to the eye. The two sets are identical within the experimental error. The slope difference for alkanes, and double its value, are also shown.

is a good two-dimensional powder. Indeed, the GID peak widths broaden considerably, and correspond to coherence lengths of a few hundred Å only. This drastic reduction in the crystalline domain size is probably related to strains introduced by the molecular tilt, as also observed in Langmuir monolayers of surfactants on water [22]. The hydrogen bonding may also have an influence on the reduction in the coherence lengths, since in I the tilted phases of the surface-frozen monolayer of alkanes do not show any reduction in the coherence length as compared to the untilted ones.

Finally, only $C_{28}OH$ shows two in-plane peaks, given in Fig. 5(a). The separation of the two peaks is small: $\Delta q_{\parallel} \approx 0.02$ Å^{-1}. This indicates a very slightly distorted hexagonal packing, though the tilt direction remains the same: next-nearest neighbors, as for all other tilted alcohols ($n \geqslant 24$). This crystalline packing may, again, indicate a different surface phase, as mentioned above.

b. *Bragg rod measurements*. The intensity distribution along q_z at each in-plane ($q_{\parallel}$) peak position, the so-called Bragg rods (BR's), have been measured with a linear position sensitive detector, placed vertically behind the Soller slits. From the BR's one can deduce the molecular tilt. The BR, shown in Fig. 5(b), is determined by the product of the molecular form factor and the structure factor of the hexagonally packed bilayer. The structure factor consists of lines along the surface normal, while the form factor is dependent on the molecular shape. In our case, it is symmetric relative to the molecular axis, which is not necessarily directed along the surface normal. Wave-vector components along (normal to) the *molecular axis*, denoted Q_z ($Q_{\parallel}$), and those along (normal to) the *surface normal*, denoted q_z ($q_{\parallel}$), are related by

$$Q_z = q_z \cos\theta - q_x \sin\theta, \tag{1}$$

$$Q_{\parallel} = \sqrt{q_y^2 + (q_z \sin\theta + q_x \cos\theta)^2}, \tag{2}$$

with θ being the tilt angle away from the surface normal [6,15], $q_x = |\vec{G}_{hk}| \cos\psi_{hk}$ and $q_y = |\vec{G}_{hk}| \sin\psi_{hk}$, where $\vec{G}_{hk}$ is

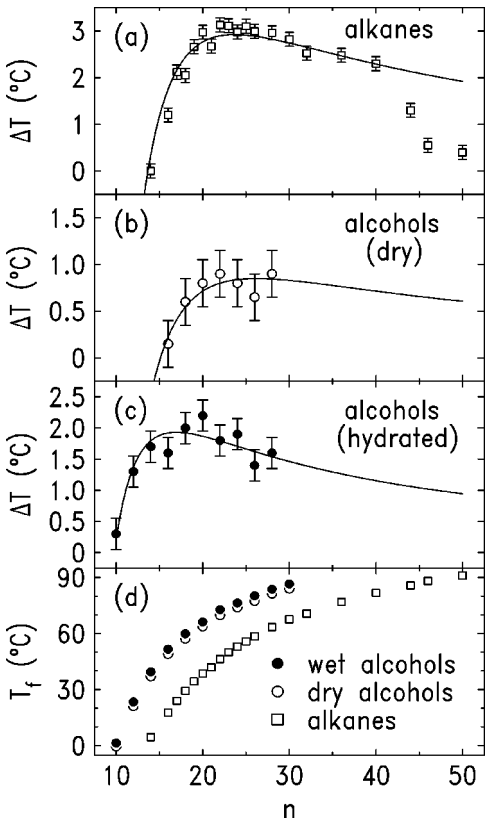

FIG. 7. The temperature range of existence of the surface crystalline phase ΔT vs chain length n, for the dry (b) and hydrated (c) alcohols, and, for comparison, for alkanes (a). The lines are fits to the $\Delta T = a/n - b/n^3$ expression shown to hold for alkanes. The relevant bulk freezing temperatures are shown in (d).

the reciprocal lattice vector considered and ψ_{hk} is the angle from the molecular tilt direction to $\vec{q}_{\parallel} = \vec{G}_{hk}$. The Form factor is peaked at $Q_z = 0$, or equivalently at $q_z = |\vec{G}_{hk}| \tan\theta \cos\psi_{hk}$. For chain molecules of length d, the form factor is $F(Q_{\parallel}, Q_z) \sim \sin(Q_z d/2)/(Q_z d/2)$. Our surface layer is a bilayer, and we find that in order to obtain a good fit to the BR data it is necessary to allow for a shift $\vec{\delta}_{\parallel}$ between the lattices of the upper and lower layers. In all fits we find that the molecules of the lower layer reside in the ''hollows'' between the hexagonally-packed molecules of the first layer. As shown in the inset of Fig. 5(b), there are two possibilities for such an arrangement with $\vec{\delta}_{\parallel,1} = (2\vec{a}_1 + \vec{a}_2)/3$ (open circles) and with $\vec{\delta}_{\parallel,2} = (\vec{a}_1 + 2\vec{a}_2)/3$ (open squares), where $\vec{a}_{1,2}$ are the lattice vectors of the upper layer (solid circles). Thus, interference between waves diffracted from the upper and lower layers will modify the Bragg rods due to the difference in the optical path lengths, and the rod profile will be given by [14,15]

$$I(q_z) \propto \left[\left(\frac{\sin(Q_z d/2)}{Q_z d/2} \right)^2 e^{-(Q_z \sigma_0)^2} \right] e^{-(q_z \sigma)^2} \times \left| 1 + C e^{-i\vec{q}_z \cdot \vec{d}} (e^{-i\vec{q}_{\parallel} \cdot \vec{\delta}_{\parallel,1}} + e^{-i\vec{q}_{\parallel} \cdot \vec{\delta}_{\parallel,2}})/2 \right|^2 |T(\beta)|^2. \tag{3}$$

Here $\exp[-(Q_z\sigma_0)^2]$ represents the decay of the molecule's electron density at its two ends, $\exp[-(q_z\sigma)^2]$ accounts for

the surface roughness, and $|T(\beta)|^2$ is the surface enhancement factor [23], which is about 4 for exit at a grazing angle $\beta \approx \alpha_c$, and approaches unity for $\beta \gg \alpha_c$. $C = \exp[-(q_\parallel \sigma_\parallel)^2/2]$ represents thermal fluctuations in the shift $\delta_\parallel$, with a Gaussian distribution width $\sigma_\parallel$. In all our fits $\sigma_\parallel \sim 0.5$ Å, so that $C \sim 0.75$, virtually independent of n. $|1 + C\exp(-i\vec{q}_z \cdot \vec{d})[\exp(-i\vec{q}_\parallel \cdot \vec{\delta}_{\parallel,1}) + \exp(-i\vec{q}_\parallel \cdot \vec{\delta}_{\parallel,2})]/2|^2$ includes a phase factor due to the shift between the upper and lower layers' lattices, assuming equal probabilities for the two nonequivalent shifts of the lower layer relative to the upper one. Note that this term does not appear in the equivalent expression for a monolayer [compare Eq. (11) in I]. For surface-normal molecules $Q_z = q_z$, $Q_\parallel = q_\parallel$ and $\vec{q}_z \cdot \vec{d} = q_z d$. Thus the form factor, and the rod intensity, have their maximum at $q_z = 0$, i.e. at the plane of the surface. For a hexagonal lattice, the six lowest-order in-plane reflections $\vec{G}_{(\pm 1,0)}$, $\vec{G}_{(0,\pm 1)}$, and $\pm \vec{G}_{(1,\pm 1)}$ have identical Bragg rods, with $\vec{G}_{(1,0)}$ and $\vec{G}_{(0,1)}$ being the primitive reciprocal lattice vectors.

The Bragg rods for $18 \leqslant n \leqslant 22$ are well fitted [solid lines in Fig. 5(b)] by a model assuming molecules aligned along the surface normal, although tilts of $\lesssim 5°$ cannot be excluded. Note that the nonzero BR peak positions observed, $q_z \approx 0.1$ Å^{-1}, do not result from a tilt, as in the case of a monolayer (see Fig. 8 in I), but rather from interference between waves reflected from the upper and the lower layers. The second-layer molecules are found to reside in the hollows of the first-layer ones. The molecular lengths obtained from the fits agree well with, though are somewhat ($\leqslant 2$ Å) shorter than, those derived from the reflectivity measurements.

For $n \geqslant 24$, the rather large nonzero peak position of the BR indicates that the molecules are tilted. In this case, not all six lowest-order BRs are identical. One of the high-symmetry tilt direction is toward a nearest neighbor [24]. This is found, for example, in the surface-frozen crystalline monolayer of long chain *n*-alkane melts [6]. Such a tilt direction yields one BR peak at $q_z = 0$, for $\vec{G}_{(\pm 1,0)}$, and another at a finite $q_z = |\vec{G}_{(0,1)}| \cos 30° \tan\theta$, for $\vec{G}_{(0,1)}$ and $\vec{G}_{(-1,1)}$. The absence of a $q_z = 0$ peak in the measured BR's for $n \geqslant 24$ [Fig. 5(b)] excludes the possibility of the nearest-neighbor tilt direction here. Another high-symmetry tilt direction is toward the next-nearest-neighbor. For this structure, the first-order peaks splits into two groups, both at nonzero q_z. One is at $q_{z1} = |G_{hk}| \cos 60° \tan\theta$, for $G_{(1,0)}$ and $G_{(-1,1)}$, and the other is at $q_{z2} \approx 2q_{z2} = |G_{hk}| \tan\theta$, for $G_{(0,1)}$. Note, however, that unlike the cases of surface-frozen layers of *n*-alkanes [6] and Langmuir films on water [25], which are both *mono*layers, in our case the interference between the waves originating at the two layers of the bilayer will modify both the positions and the intensities of these two peaks, as already discussed above for the nontilted phase. The low-order peak q_{z1} [see Fig. 5(b)] is clearly observed in the experiments. It shifts to higher q_z with increasing n, indicating an increasing tilt angle. A fit of Eq. (3) above to the measured BR yields the tilt angles listed in Table I. Note that in spite of an extensive search of the $(q_z, q_\parallel)$ plane no q_{z2} peaks were found for the significantly tilted $C_{24}OH$ and $C_{26}OH$, although for $C_{28}OH$ a prominent q_{z2} peak was observed, and is shown in Fig. 5(b). Without observations of the second BR peak positions and their corresponding $q_\parallel$, one cannot exclude the possibility of a distorted-hexagonal structure for $n = 24$ and 26. Also, the area and molecule and the distortion parameter ξ cannot be determined [26].

For $n = 28$ a behavior different from that of $n = 24$ and 26 is observed. The $C_{28}OH$ data display two peaks at $q_{z1} = 0.24$ Å^{-1} and $q_{z2} = 0.47$ Å^{-1}, and a slightly different $q_\parallel$, as discussed above. This is consistent with a distorted hexagonal packing, and a next-nearest-neighbor tilt. A detailed analysis, using Eqs. (2)–(4), yields a fitted chain length of $d = 33.0 \pm 1$ Å, close to, but about 1.6 Å shorter than, the chain length obtained from the reflectivity measurements. More importantly, the fitted tilt angle, $\theta = 17°$, is *smaller* than that of $C_{26}OH$. This is contrary to the trend of an increasing tilt with chain length as long as phase boundaries are not crossed. This trend was observed in I for alkanes, and also here for $22 \leqslant n \leqslant 26$. By contrast, when crossing a phase boundary, a jump in the tilt angle, and sometimes also in the tilt direction, may occur as found for C_{44} alkane in I, and for alkane mixtures [27]. The tilt jump from $C_{26}OH$ to $C_{28}OH$, supports, therefore, the suggestion, discussed above, of a rotator-to-crystal surface phase transition at this point. Additional support for this suggestion is obtained from the fact that the q_{z2} peak is not observed for $n = 24$ and 26, while it is rather prominent for $n = 28$. As q_{z2} and the corresponding Q_{z2} are rather large, the exponential roughness terms $\exp[-(q_z\sigma)^2]$ and $\exp[-(Q_z\sigma_0)^2]$ will have a substantial effect on the peak intensity. The trend observed may result from a large reduction in the roughness upon moving from $n = 26$ to $n = 28$. This is in line with the considerably larger axial disorder of the rotator phase [7–9,20], as compared with that in the crystalline phase. The conclusion of a rotator-to-crystal phase transition here is further supported by the reduced roughness parameter observed for $C_{28}OH$ in the reflectivity measurements, discussed above. For $C_{28}OH$ we obtain a molecular-axis-normal area per molecule, $A = 20.5$ Å^2, and a distortion parameter $\xi = 0.031$. Comparing these to the untilted molecule, where $A = 20.26$ Å^2, we find a very small *increase in A*. This is in contrast to alkanes, where *A decreases* from ~ 19.7 to 18.7 Å^2 in the surface rotator-crystal transition. Also, the distortion parameter is much smaller than that of the crystalline surface monolayer of C_{44} alkane, $\xi = 0.112$, and is closer to that of bulk R_{IV} rotator phases [4,17,28]. These differences may result from the different tilt directions in alkanes and alcohols, from the bilayer vs monolayer structure, or all these differences may indeed have a common source, presumably the HB which exists in alcohols but not in alkanes. Clearly, further studies on a wider range of chain molecules are called for to fully understand the interplay between the interactions and structure in the surface-frozen layer.

3. Thermodynamical properties

The surface tension γ measured for $C_{22}OH$ as a function of temperature is shown in Fig. 3(b). By comparison to the T scan, discussed above, in Fig. 3(a) the formation of the bilayer can be observed as the clear cusp at T_s. At this temperature the slope of γ changes abruptly from a small negative value for $T > T_s$, typical of simple liquids, to a large

positive value for $T<T_s$. This change is a clear indication of the formation of an ordered surface layer on top of the bulk liquid, as discussed in I for *n*-alkanes [6], and also for sodium dodecyl sulfate (SDS)–water lyotropics [29], and liquid metals [30]. Since γ is the excess free energy per unit area of the surface over that of the bulk [13], it can be written as

$$\gamma=\epsilon'-T(S'-S)=\epsilon'-T\delta S, \tag{4}$$

where ϵ' is the excess surface energy per unit area, and S' and S are the entropy densities in the surface layer and the bulk liquid, respectively. For the normal liquid surface at $T>T_s$ the surface molecules are less constrained than those in the bulk and thus S' is larger than S, yielding $d\gamma/dT=-(S'-S)<0$. As the surface freezes at $T=T_s$ the surface molecules become more constrained than those in the liquid bulk so that $S'\ll S$, leading to $d\gamma/dT=-(S'-S)>0$. The abrupt change of slope seen in Fig. 3(b) suggests, again, a first-order transition, to within the few m °C experimental resolution. The absence of any further slope changes implies that no further layering occurs down to bulk freezing, in full agreement with the x-ray T scan shown in Fig. 3(a) and discussed above.

The slope for $T>T_s$ is relatively small and independent of n, whereas the slope for $T<T_s$ is larger and significantly n dependent. For all alcohols we obtain $(d\gamma/dT)_{T>T_s}=-0.09\pm0.01$ mN m^{-1} °C^{-1}, consistent with the literature values [5,31], and close to the values obtained for alkanes. By contrast, the slope for $T<T_s$ increases significantly with n. Denoting the slope difference above and below T_s by

$$\Delta(d\gamma/dT)=(d\gamma/dT)_{T<T_s}-(d\gamma/dT)_{T>T_s} \tag{5}$$

$$=-(S'_{T>T_s}-S'_{T<T_s})=\Delta S_s, \tag{6}$$

where ΔS_s, the surface entropy difference between the liquid and frozen phases, is defined by the last equation. The experiment shows a linear dependence on n, namely, $\Delta S_s\equiv\Delta(d\gamma/dT)_{\rm expt}=(-0.37+0.11)n$ mJ m^{-2} °C^{-1}. Using the values from I, we obtain for *n*-alkanes $\Delta S_s=\Delta(d\gamma/dT)_{\rm expt}=(-0.054+0.06)n$ mJ m^{-2} °C^{-1}, i.e., roughly half that of alcohols. This is as expected, since the surface layer in alcohols is a bilayer, and in alkanes a monolayer. In Fig. 6 we plot $\Delta S_s=\Delta(d\gamma/dT)_{\rm expt}$ for alkanes and alcohols. This quantity is proportional to the loss in the number of degrees of freedom upon chain freezing. For alkanes, the surface values are consistent with those of the corresponding bulk rotator phases, extracted from the latent heat and melting temperature measurements [4–6], and normalized to a single molecular layer and a unit area. For bulk alcohols, the entropy change in the liquid-rotator transition is [17] $\Delta S_b=(-0.58+0.138)n$ mJ m^{-2} °C^{-1}, close to, but systematically larger by $\sim$20% both in magnitude and in the slope, than that of the surface, ΔS_s. This may be due to a slightly larger disorder of the chain ends (on the vapor and liquid sides) in the surface-frozen bilayer, as compared to chains included in a bilayer residing in the bulk, where the molecules are more confined. As can be seen in Fig. 6, the slopes of the linear fits to the measured ΔS_s values are very close for $\Delta S_s^{\rm alcohol}$ and $2\times\Delta S_s^{\rm alkane}$. This demonstrates that the n variation of ΔS_s comes in both cases from the chain, and not from changes in the headgroups, as indeed expected. Figure 6 also shows that $\Delta S_s^{\rm alcohol}<2\times\Delta S_s^{\rm alkane}$ systematically. This can be understood by assuming that a few CH_2 units adjacent to the OH groups remain ordered even in the liquid phase due to the stabilizing effect of the HB network. Hence the reduction in entropy upon surface freezing is obtained from less than the full chain length n. A similarly reduced entropy gain per chain was observed in alcohols for the bulk liquid-rotator transition [17] and in Langmuir monolayers of alcohols on water [17,32,33], where the entropy reduction is even further diminished by the enhanced HB due to the water subphase. The downshift in n required to bring the ''alcohols dry'' line in Fig. 6 to overlap the ''alkanes $\times$ 2'' line is a rough estimate for the number of ordered CH_2 units per two alcohol molecules (because of the bilayer structure). From Fig. 6 this can be estimated as $\sim$3.6 or about 1.8 ordered CH_2 units per molecule. This is less then, but similar to the $\sim$3 ordered CH_2 units estimated for the three-dimensional bulk [17] from the extrapolated intercept of the liquid-rotator transition entropy ΔS vs n with the $\Delta S=0$ axis. While an intercept analysis in our case is less accurate because of the larger error bars and limited n range, it yields $\sim$1.6 ordered CH_2 units, in good agreement with the shift method result. The near-headgroup CH_2 ordering in our case is expected to increase upon hydration due to the enhancement of HB, which is reflected in the increase in T_f and T_s. This may account for the fitted ''alcohols wet'' ΔS_s line being slightly lower than the corresponding dry one in Fig. 6. This is further discussed below. Finally, note that in I the rotator-to-crystal phase transition in the surface-frozen monolayer in alkanes at $n=44$ was accompanied by a large change in ΔS_s, due to the freezing out of the rotational degrees of freedom. The absence of such a change in Fig. 6 for $n=28$ argues against the suggestion, made above, of a similar phase transition in the surface bilayer in alcohols.

4. Surface phase diagram

Surface freezing does not occur for all chain lengths n. In dry alcohols it is observed for $16\leqslant n\leqslant 28$ only. Moreover, it has only been observed for even carbon numbers. This is in contrast with alkanes, where odd-even effects are not observed either in the occurrence of the effect or in the temperature range of existence $\Delta T(n)$. This is in line with the alkane bulk behavior, where no odd-even effects were observed in the transition temperatures of the liquid-rotator phase transitions for the n range under discussion [4]. The absence of surface freezing in odd alcohols cannot be attributed to the preemption of surface freezing by bulk freezing, since no odd-even effects occur in the bulk liquid-rotator transition temperatures in alcohols [17]. While the rotator-crystal bulk transition does show an odd-even effect, the transitions for odd carbon numbers occur at temperatures *lower* than those extrapolated from their neighbouring even ones. This results in a larger temperature range for the less-ordered rotator phase, indicating a reduced tendency for ordering. The preference of the surface of odd alcohols to stay in the disordered liquid phase rather than form an order bilayer may be another reflection of the same tendency. On a

molecular level, the reason for the odd-even effect in surface freezing is most likely related to differences in the orientation of the terminal OH group relative to the molecular axis, which may render the formation of HB unfavorable in odd alcohols by making the relevant HO···H distances much different from the optimal ~2.8 Å of this bond [34]. Langmuir monolayers of alcohols, and some of their derivatives, on water were shown to have considerably different terminal hydroxyl group orientations for odd and even chain lengths. This difference was claimed to be the cause for the large odd-even effect in the efficiency of these Langmuir monolayers as ice nucleators from supercooled water [22,34,35]. It is true that analogies from effects observed in Langmuir monolayers on water to surface freezing in general, and to our bilayers in particular, have to be drawn with caution, as discussed in Sec. I C in I. This is particularly true for alcohols, because of the considerably different structure (packing, tilt magnitude and direction, crystalline rather than rotator, etc.) of those monolayers from the bilayer observed here. Nevertheless, it is highly likely that the orientation of the hydroxyl group is the common cause of the odd-even effects in both systems. To date very few studies addressed these orientations in the bulk, and none of them for the rotator phases, which are most relevant for surface freezing.

The $(n,\Delta T)$ phase diagrams of alcohols for even carbon numbers, both dry and hydrated, have been derived from both the surface tension and the x-ray measurements, and are shown in Figs. 7(b) and 7(c). For comparison, Fig. 7(a) shows the same phase diagram for alkanes. As for alkanes, the nonmonotonic n dependence is due to the competition between energy and entropy, as discussed in detail for liquid alkanes in I: while energy terms increase with n and thus drive for more order and a larger ΔT, the increasing entropy terms drive for less order and thus for a smaller ΔT range. The more complex interactions in alcohols, which now include HB between molecules in the two layers, result in a balance different from that of alkanes, and as can be seen in the figure, reduce considerably both the temperature ΔT ($\leqslant 1\,^{\circ}\mathrm{C}$ vs $3\,^{\circ}\mathrm{C}$) and the n ($16 \leqslant n \leqslant 28$ vs $16 \leqslant n \leqslant 50$) ranges of existence, relative to alkanes. The relation $\Delta T = a/n - b/n^3$, found to be valid (with $a = 103.8$, $b = 19393.5$) for alkanes in I, agrees with ΔT for alcohols as well, both dry ($a = 33.4$, $b = 7628.8$) and hydrated ($a = 49.1$, $b = 4701.6$), as shown by the lines in Figs. 7(a)–7(c). It gives a characteristic increase from zero at the low-n end of the diagram. The occurrence of this end at $n \approx 14$ for both alcohols and alkanes may be a coincidence, in view of the different structure of the surface layer. For alkanes, the fall-off at the high-n end of the phase diagram, faster than that predicted by the empirical ΔT above, was ascribed in I to the strains accompanying the rotator-to-crystal transition in the surface layer at $n = 44$. The even more abrupt disappearance of the surface phase in alcohols for $n = 30$ may well have a similar origin, and supports the possibility of a rotator-to-crystal phase transition in the surface bilayer at $n = 28$, as discussed above [36]. The implications of the considerable reduction upon hydration of the low-n limit (from $n = 16$ to 10), observed in Fig. 7(c), while leaving the high-n limit unchanged, at $n = 30$, are discussed in Sec. III B. The bulk freezing temperatures T_f vs n for the alcohols showing surface freezing are plotted in Fig. 7(d). This demonstrates the much larger range of T_f values for the alkanes, as compared to alcohols, and the *increase* in T_f in hydrated alcohols, also discussed in Sec. III B.

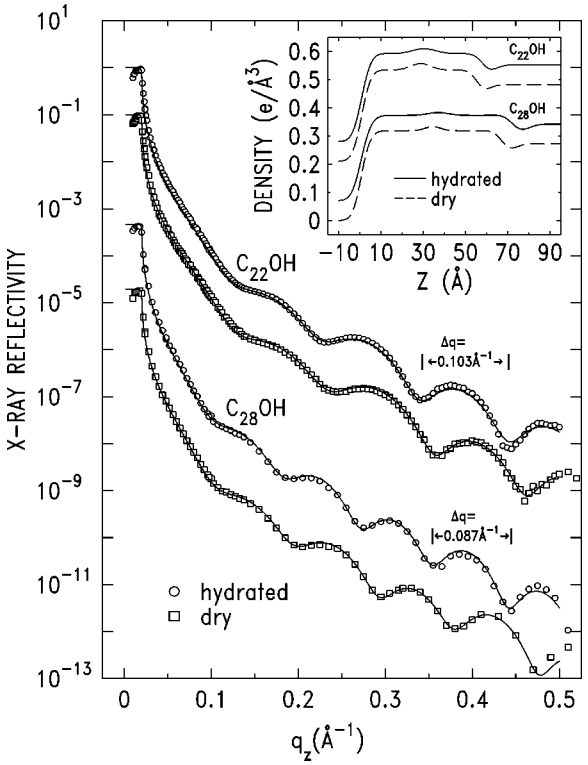

FIG. 8. X-ray reflectivity measurements for dry (squares) and hydrated (circles) alcohols. Note the decreased modulation periods Δq (marked on the figure) of the hydrated samples, indicating swelling. The corresponding electron density profiles are shown in the inset.

B. The hydrated alcohol melt

To obtain a better assessment of the role of HB's in the formation, the thermodynamics, and the structure of the surface bilayer, we have done x-ray and surface tension measurements on hydrated alcohols. This study was also part of a program exploring the possibility of controlling the thermodynamics and structure of surface-frozen layers by bulk additives [37,38]. The hydrated alcohols were found to exhibit surface freezing over considerably larger n and ΔT ranges than the dry alcohols. As for dry alcohols, no surface freezing was observed in hydrated alcohols with odd n. We now present the results obtained by these measurements and compare them to those obtained for dry alcohols.

1. Surface-normal structure

Figure 8 compares the XR curves measured for dry and hydrated $C_{22}OH$ and $C_{28}OH$ in their surface-frozen phase. Clearly, the bilayer structure is preserved upon hydration. The periods of the modulations observed for these two hydrated alcohols, $\Delta q_z^{\mathrm{wet}} \approx 0.103$ and 0.087 $\mathrm{Å}^{-1}$ are somewhat smaller than the $\Delta q_z^{\mathrm{dry}} \approx 0.108$ and 0.090 $\mathrm{Å}^{-1}$ of the same dry alcohols. The hydrated layer thicknesses estimated from the modulation periods, $D^{wet} \approx 60.8$ and 72.2 Å, are 2–2.5 Å larger than the corresponding dry values $D^{\mathrm{dry}} \approx 58.2$ and 70

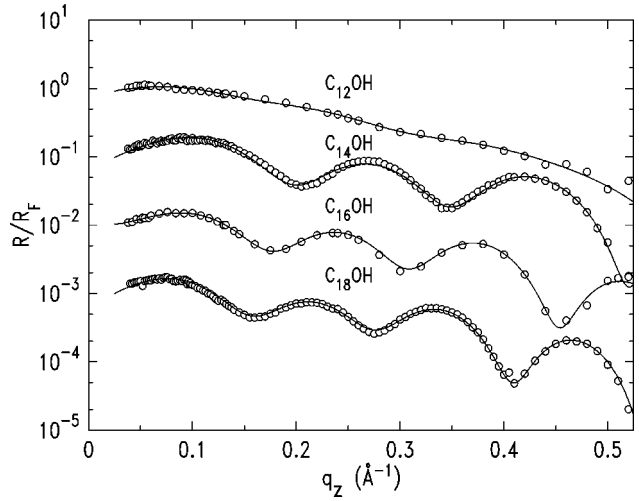

FIG. 9. X-ray reflectivity, normalized to the Fresnel reflectivity R_F, for several hydrated alcohols in the surface-frozen phase. The two shortest alcohols do not show surface freezing when dry, and $C_{16}OH$ has only a very small $\Delta T = 0.15\,^{\circ}C$ when dry, but nearly 2 °C when wet. The lines are fits to the model discussed in the text.

Å. The magnitude of this swelling, its n independence, and its appearance for nontilted molecules like $C_{18}OH$, indicate that it is not due to a mere variation in the molecular tilt, but rather to a more profound structural change. Following similar studies of bulk rotator phases in alcohols [17], an intercalation of water molecules in the center of the surface bilayer seems a very likely cause for the swelling. The increase upon hydration in the n range of the alcohols showing surface freezing, discussed below, allowed for XR measurements on $n = 12$ and 14, which do not show surface freezing when dry. The measured reflectivity curves, normalized to R_F, are shown in Fig. 9. Note that while for $C_{14}OH$ a good contrast between maxima and minima is observed, for $C_{12}OH$ a poor contrast was obtained, indicating an incomplete coverage (only 20–25 %) of the surface by the surface-frozen layer. Nevertheless, the length determined from the modulation period of that curve, as well as from the other reflectivity curves shown, including $C_{14}OH$, are consistent with a fully extended molecule, oriented normal to the surface, as expected from the XR and the BR results obtained for dry alcohols in this n range.

To pinpoint the structure, we have fitted the XR curves by the same four-layer model discussed above for the dry alcohols, taking the values refined for dry alcohols as starting values for all parameters. As shown in Figs. 8 and 9, excellent fits were obtained, even for the low-contrast $C_{12}OH$ curve. All parameter values remained, within the fit error, the same as those of the dry alcohols except for a systematic increase in the thickness of the OH layer by 2.4–2.7 Å, and an increase in the roughness at the bilayer-vapor surface by ~0.6 Å. The fitted layer thicknesses are listed in Table II, along with other structural and thermodynamic properties of the hydrated surface layer. The swelling is ~0.5 Å larger then that observed in the corresponding *bulk* rotator phase of hydrated alcohols [17]. A direct integration over the surface electron density profiles yields ~14 additional electrons in the OH layer per molecular area (~20 Å) upon hydration. This is slightly more than, though close to, the ten electrons

TABLE II. Same as Table I, but for hydrated alcohol melts.

n	$D/2$ (Å)	$q_\parallel$ (Å^{-1})	q_z (Å^{-1})	θ (°)	T_f (°C)	ΔT (°C)	ΔS_s (mJ m^{-2} K^{-1})
12	17.91				23.4	1.7	0.82
14	20.38				39.5	1.7	1.28
16	23.38				51.6	1.8	1.38
18	25.72	1.48	0.1	<5.0	59.9	2.0	1.7
20					66.5	2.0	1.6
22	30.41	1.47	0.09	<5.0	72.8	1.8	1.95
24					76.35	1.9	1.8
26					80.2	1.4	2.8
28	37.16	1.46	0.2	19.0	83.7	1.6	2.45
30					86.5		

(or a single water molecule) found for the bulk [17]. Note that due to the bilayer structure of both the surface-frozen and bulk rotator phases, this corresponds to an approximately 1:2 water-alcohol molecular ratio.

The layer's half-thickness d obtained from the XR fits are shown in Fig. 4(a). Note their consistently 2.5 Å larger thickness, compared to the dry alcohol, as mentioned above. To within the fit error, the slope of $d(n)$ is the same as that of the dry alcohols, indicating that, apart from the swelling, no major changes occur in the structure of the bilayer such as a change in the tilt and/or conformation of the chains. Since the liquid-vapor surface roughness σ_1 is an important diagnostic tool for phase changes, as discussed above, we have repeated the XR fits using a single roughness parameter σ for all interfaces of the model, as done above for the dry alcohols, to allow an accurate assessment of the roughness variation with n. The results obtained are plotted in Fig. 4(b). Aside from the $C_{12}OH$ result, which is anomalously high because of the imperfect surface layer, all values follow the same trend of the dry alcohols. σ^{wet} seems to be slightly higher than σ^{dry}, although the difference is within the combined measurement errors. This higher roughness may be indicative of an enhancement of the bilayer's rotator nature, a dominant characteristic of which is a high axial disorder [20]. The roughness change upon hydration, observed in the figure, for $C_{28}OH$ is significant. If the surface bilayer of the dry $C_{28}OH$ can be considered to be crystalline, rather than rotator, as discussed above, then this increase in σ, and the agreement with the value extrapolated from the lower-n alcohols, all of which have rotator bilayers, can be interpreted as indicating that the hydrated $C_{28}OH$ is also a rotator. Although this evidence is by no means conclusive, further support for this suggestion is provided by the BR measurements discussed below.

The T scan shown in Fig. 3(a) demonstrates that, similar to dry alcohols, the surface freezing of hydrated alcohols is a first-order effect, to within a few m °C. The constant intensity below T_s indicates that no further layers are formed, and no changes occur in the bilayer down to T_f. The considerable increase upon hydration in the temperature range of existence ΔT observed in both surface tension and T-scan measurements presented in Fig. 3 is discussed below in detail.

2. Surface-parallel structure

The GID and BR measurements are shown in Fig. 10 for two hydrated alcohols. As a comparison of the $q_\parallel$ and q_z

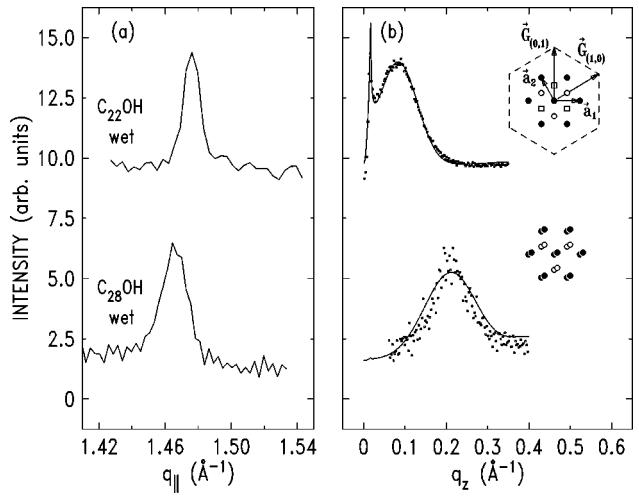

FIG. 10. Same as Fig. 5, but for the hydrated alcohols indicated. Note that only a single in-plane peak and a single Bragg rod peak are now observed for $C_{28}OH$, indicating that hydration may induce a transition to a rotator surface phase for this compound.

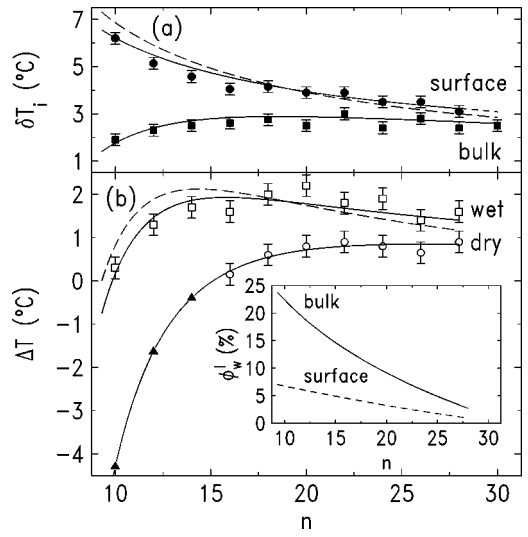

FIG. 11. (a) The increase δT_i, measured (points) and calculated (lines), in the surface and bulk freezing temperatures upon hydration. The dashed ''wet'' line assumes *n*-independent hydration of the surface-frozen bilayer, and the solid line a linearly *n*-dependent one. (b) The corresponding temperature ranges of existence of the surface freezing. The solid and dashed ''wet'' lines correspond to the same lines in (a), respectively. Note the excellent agreement of the solid lines with the measured data in both (a) and (b). The effect vanishes for $n=30$, hence no points are shown for this n. The inset shows the molar fraction of water in the *liquid* surface phase (dash line) as derived, using the modified Gibbs adsorption rule, from the corresponding *liquid* bulk value (solid line), extrapolated from previously measured data [41].

values for $n=18$ and 22 in Tables I and II reveals, a small $\sim 2\%$ in-plane lattice expansion occurs upon hydration. The observation of a single GID peak with a low-q_z BR peak for $n=18$ and 22 indicates that the packing remains hexagonal, and the molecules untilted. Note that in the bulk rotator phase of the same molecules no change was observed in the in-plane spacing upon hydration [17]. The in-plane temperature expansion coefficient, observed to be anomalously large in the bulk [17], could not be determined here due to the limited range of existence ΔT of the surface bilayer. For the only tilted surface phase measured, $C_{28}OH$, no in-plane lattice expansion is observed upon hydration, but the smaller q_z position, as well as the full-rod fit shown in Fig. 10(b), indicate a slight $\lesssim 2°$ reduction in the tilt, as compared to the dry sample, but no change in the next-nearest-neighbor tilt direction. For the bulk tilted phases the tilt angle is significantly reduced by hydration, sometimes down to zero (see Table III in Ref. [17]). Note that similar to the dry $C_{24}OH$ and $C_{26}OH$ bilayers, and in contrast with the *dry* $C_{28}OH$, no high-q_z peak could be found for the *hydrated* $C_{28}OH$. The single peak implies an hexagonal packing, unlike the distorted-hexagonal of dry $C_{28}OH$. Moreover, the absence of the high-q_z peak may be assigned, as done for the dry $n=24$ and 26 rotators, to roughness due to high axial disorder, a characteristic of the rotator phases. These observations support, therefore, the suggestion above of a crystal-to-rotator phase transition upon hydration for the $C_{28}OH$ surface bilayer.

3. Thermodynamic properties and phase diagram

The measured $\gamma(T)$ curve for hydrated $C_{22}OH$ is shown in Fig. 3(b). The slope observed for $T<T_s$ is slightly smaller than that of the dry alcohol for this particular case. A comparison of ΔS for each chain length, shown in Fig. 6, indicates that within the experimental scatter (± 0.25 mJ m^{-2} °C), $\Delta S_s^{\rm wet} \approx \Delta S_s^{\rm dry}$. Nevertheless, a linear fit to all $\Delta S_s^{\rm wet}$ values results in a slightly lower line than that fitted to the measured $\Delta S_s^{\rm dry}$. Thus, the stabilizing effect that the hydration has on the bilayer is reflected in only a slight decrease in the entropy reduction upon freezing. Assume now a HB-induced residual order of a few headgroup-adjacent CH_2 groups in the dry liquid phase, as discussed above. The increase in the number of these ordered carbons upon hydration can be estimated from the *n* downshift required to bring the ''wet'' line into overlap with the ''dry'' one in Fig. 6. This is an average of ~ 1.6 carbons. The bilayer structure implies, therefore, an increase of the ordered part by slightly less than a single CH_2 unit upon hydration. This corresponds to a rather small reduction in the total vdW energy of ~ 1 kJ/mol upon hydration. Another, more prominent, manifestation of the increased stability is the significant *increase* in both T_f and T_s upon hydration, shown in Fig. 11(a). This is in contrast with the *decrease* observed in the bulk freezing temperatures of alcohols and alkanes with increasing non-aqueous impurity concentration, as demonstrated, for example, in binary mixtures of different-length alkanes [27] and alcohols [39].

Figure 11(a) shows the considerable increases, $\delta T_s = T_s^{\rm wet} - T_s^{\rm dry}$ and $\delta T_f = T_f^{\rm wet} - T_f^{\rm dry}$, in T_f and T_s, respectively, upon hydration. The increases are found to be unequal, with $\delta T_s > \delta T_f$ for all n, so that the temperature range of existence, $\Delta T^{\rm wet}$, becomes up to twofold larger than $\Delta T^{\rm dry}$. δT_f is approximately constant with n at ~ 2.5 °C, and agrees closely with other bulk measurements [17]. δT_s, however, varies by a factor of 2 and decreases from ~ 6 °C for $n=10$ to ~ 3 °C for $n=28$. As shown in Fig. 11(b), the vanishing of the surface freezing (SF) effect at $n=30$ [36] persists upon hydration. However, the low-n limit of the SF effect is decreased considerably, down to $n=10$. This in-

creases the n-range of existence of the SF effect by $\sim 50\%$.

The dramatic increases in T_f, T_s and the n range can be accounted for quantitatively, by considering the hydration levels of the bulk and the surface, and taking into account the differences in that level due to adsorption or depletion of water at the surface, as predicted by the Gibbs rule [40] appropriately modified for the case at hand. The detailed discussion of the calculations, given below, is divided for calrity into separate sections.

(a) Consider first the hydrated alcohol. In the alcohol-water binary mixture, the excess free energy per molecule at the surface is $f=\epsilon - T\delta S$, where ϵ is the energy and δS is the entropy difference between surface and bulk. For a mixture of N alcohol molecules and M water molecules, and assuming a negligible alcohol-water repulsion term, the free energy at the surface is

$$F = Nf_a + Mf_w + Nk_BT \ln \phi_a + Mk_BT \ln \phi_w \tag{7}$$

where the subscripts w and a indicate water and alcohol, respectively, and ϕ_w and $\phi_a = 1 - \phi_w$ are the corresponding molar fractions in the mixture. The chemical potentials of the alcohol at the liquid (l) and rotator (r) phases at the surface are given by $\mu^l_{a,s} = \partial F/\partial N = f^l_{a,s} + k_BT \ln(1-\phi^l_{w,s})$ and $\mu^r_{a,s} = f^r_{a,s} + k_BT \ln(1-\phi^r_{w,s})$, respectively. Also, $f^l_{a,s} - f^r_{a,s} = \Delta\epsilon - T(\delta S^l - \delta S^r) = \Delta\epsilon - T(S^l_s - S^r_s) \equiv \Delta\epsilon - T\Delta S_s$, where $\Delta\epsilon = \epsilon^l_s - \epsilon^r_s$, S^l_s and S^r_s are the *surface* entropies in the liquid and surface-frozen rotator phases, and ΔS_s is the entropy change in the surface phase transition. The equality of the chemical potentials, $\mu^l_{a,s} = \mu^r_{a,s}$, at the surface freezing temperature $T^{\rm wet}_s$ yields

$$\Delta\epsilon + k_BT^{\rm wet}_s \ln(1-\phi^l_{w,s}) = T^{\rm wet}_s \Delta S^{\rm wet}_s + k_BT^{\rm wet}_s \ln(1-\phi^r_{w,s}). \tag{8}$$

(b) For the dry surface, $M=0$ and $\phi_w = 0$, $\phi_a = 1$, so that $\mu = \partial F/\partial N = f$ and the procedure above yields at the surface freezing temperature, $T^{\rm dry}_s$, $f^{l,{\rm dry}}_{a,s} = f^{r,{\rm dry}}_{a,s}$. This, in turn, gives $\Delta\epsilon = T^{\rm dry}_s \Delta S^{\rm dry}_s$. Making the assumption that the difference in the energy of the molecule between the liquid and rotator phases of the molecule remains unchanged upon hydration, we can substitute $\Delta\epsilon$ in the last equation, and obtain

$$T^{\rm dry}_s \Delta S^{\rm dry}_s + k_BT^{\rm wet}_s \ln(1-\phi^l_{w,s}) = T^{\rm wet}_s \Delta S^{\rm wet}_s + k_BT^{\rm wet}_s \ln(1-\phi^r_{w,s}). \tag{9}$$

(c) Experimentally, $\Delta S^{\rm dry}_s = \Delta S^{\rm wet}_s$ (see Fig. 6). Thus, denoting $\delta T_s = T^{\rm wet}_s - T^{\rm dry}_s$, we finally obtain

$$\delta T_s = k_BT_s \ln[(1-\phi^l_{w,s})/(1-\phi^r_{w,s})]/\Delta S_s, \tag{10}$$

where s denotes the surface. This is the expression for the shift δT_s in the surface freezing temperature T_s. An identical expression, with b (for ''bulk'') replacing s, can be obtained for the shift δT_f in the bulk freezing temperature T_f. Both depend on the respective molar concentrations of water in the liquid and rotator phases $\phi^{l,r}_{w,i}$ of the surface ($i=s$) and of the bulk ($i=b$). Unequal hydration levels in the bulk and the surface in one or both phases will results in unequal shifts for the freezing temperatures. The observation of unequal shifts indicates, therefore, that different hydration levels indeed exist at the surface and bulk in the liquid and rotator phases.

To calculate δT_f and δT_s as a function of n from the equations above, and compare them with the measured values, we need to know $\phi^l_{w,i}$, $\phi^r_{w,i}$ and ΔS_i for the bulk ($i=b$) and the surface ($i=s$). Note that, according to Eq. (10), to obtain $\delta T_{s,f} > 0$, as observed, we must have $\phi^l_{w,i} < \phi^r_{w,i}$. The required quantities were obtained as follows.

(i) For the bulk, the water concentration in the melt, $\phi^l_{w,b}$, was measured by Lawrence *et al.* [41], and indeed shows an unusual *lower* water concentration in the liquid phase than in the solid rotator phase. Their data extend, however, up to $n=17$ only. We find that $\phi^l_{w,b}(n) = (0.663 - 0.1911)\ln(n)$, is a good functional fit to their data, which we use to calculate $\phi^l_{w,b}$ for $n>17$, and is shown in a solid line in the inset to Fig. 11(b).

(ii) From our surface tension measurements $\Delta S_s(n) \equiv \Delta(d\gamma/dT)_{\rm expt} = (-0.37 + 0.11)n$ mJ m^{-2} °C^{-1} for both wet and dry alcohols. The bulk measurements [17] show that $\Delta S_b \approx \Delta S_s$.

The calculated bulk δT_f [solid line in Fig. 11(a)] required only a slight adjustment of $\phi^r_{w,b}$ from the nominal, n-independent, $\frac{1}{3}$ (the 1:2 ratio discussed above) to 0.28 to reach the excellent agreement with the experiment seen in the figure.

(iii) For the surface, we find experimentally that $\delta T_s > \delta T_f$, which implies a *larger hydration difference* between the liquid and rotator phases for the surface than for the bulk. However, the x-ray measurements in the surface-frozen phase, discussed above, show a roughly 1:2 water:alcohol ratio, about the same as that of the bulk: $\phi^r_{w,b} \approx \phi^r_{w,s} \approx \frac{1}{3}$. The *liquid* surface must have, therefore, a lower hydration $\phi^l_{w,s}$ than the liquid bulk $\phi^l_{w,b}$ to make the hydration difference between liquid and rotator phases larger at the surface than at the bulk. To determine the bulk-surface hydration difference at the liquid phase, we use the Prigogine parallel-layer model for the surface, in the athermal approximation, where the interaction energy parameter between the two species can be neglected [42]. This yields a modified form of Gibbs' surface adsorption rule, valid for a binary mixture of different-size molecules, as is the case here [40]:

$$x^l_{w,s}/x^l_{w,b} = [(1-x^l_{w,s})/(1-x^l_{w,b})]^{1/r} \times \exp[-A_w(\gamma_w - \gamma_a)/k_BT]. \tag{11}$$

This applies in our low concentration case. x denotes the *volume* fraction corresponding to the *molar* fraction ϕ, the molecular area of water $A_w \approx 11.6$ Å^2, and $r = (1.27/1.9) \times n$ is the alcohol-water length ratio. Given the surface tension of water, $\gamma_w \approx 72$ mN/m, which is much higher than that of alcohols, $\gamma_a \approx 27$ mN/m, this rule yields concentration values from $x^l_{w,s} \approx 0.068$ for $n=10$ to $x^l_{w,s} \approx 0.01$ for $n=28$, about threefold lower than the corresponding bulk concentrations, $x^l_{w,b}$. The volume to molar concentration conversion is $\phi^l_{w,s} = x^l_{w,s}V_a/[x^l_{w,s}V_a + (1-x^l_{w,s})V_w]$, where $V_w = 30$ Å^3 and $V_a = (1.27 \times 19.5) \times n$ are the molecular volumes of the water and alcohol in Å^3, respectively. This calculation yields for $\phi^l_{w,s}$ the dash line in the inset to Fig. 11(b). It is signifi-

cantly lower than the corresponding bulk curve, as indeed expected from Gibbs' rule, in view of the higher surface tension of water as compared to that of alcohols.

Using the calculated $\phi^{l}_{w,s}$ and assuming an n-independent water concentration at the surface crystalline layer yields a good approximation to the measured δT_s, shown by a dashed line in Fig. 11(a), for a surface molar fraction of $\phi^{r}_{w,s} \approx 0.29$. This value is slightly higher than, but close to that of the bulk, discussed above, and the nominal $\sim \frac{1}{3}$ obtained from the x-ray measurements. However, relaxing the requirement of n-independent $\phi^{r}_{w,s}$ and allowing it to vary linearly with n, yields a much-improved agreement with the measured δT_s. This is shown in the ''wet'' solid line in Fig. 11(a), obtained for $\phi^{r}_{w,s} = 0.25 + 0.002 \times n$. This varies the water concentration from $\phi^{r}_{w,s} \approx 0.28$ for $n = 14$ to $\phi^{r}_{w,s} \approx 0.31$ for $n = 28$. Both these limiting values are in agreement with the nominal $\frac{1}{3}$ and the bulk value. The small variation, 10% of the surface-crystal hydration over the full n range showing SF, is not at odds with any experimental observations presented here. Moreover, it is conceivable that the increase observed in the area per molecule with n, as reflected in the decreasing $q_{\|}$ values in Table I, will facilitate the intercalation of water molecules into the bilayer and result in a slight increase in the hydration with n. The agreement of the calculated δT_i curves with the measured data in Fig. 11(a) is remarkable, in view of the simple theoretical expressions employed and the fact that virtually no adjustable parameters were used, except for the minimal change of $\phi^{r}_{w,i}$ from the nominal 1:2 value.

As observed in Fig. 11(a), $\delta T_s > \delta T_f$ for all n, which results in a considerable increase in ΔT upon hydration. This is shown in Fig. 11(b) where the solid line marked ''dry'' is the same fit to $\Delta T^{\mathrm{dry}} = a/n - b/n^3$ ($a = 33.4$, $b = 7628.8$) used in Fig. 7(b) and discussed there. Since SF does not occur in the dry sample for $n = 10$, 12, and 14, because it is preempted by bulk freezing, T_s values are not measurable for these n. These T_s values, marked by closed triangles in Fig. 11(b), were therefore extrapolated from the analytic expression above, and used in calculating the δT_s points for $n = 10$, 12, and 14 in Fig. 11(a). The ''wet'' lines in Fig. 11(b), $\Delta T^{\mathrm{wet}} = (T_s^{\mathrm{dry}} + \delta T_s) - (T_b^{\mathrm{dry}} + \delta T_f) = \Delta T^{\mathrm{dry}} + (\delta T_s - \delta T_f)$, are obtained from the calculated δT_i in Fig. 11(a), and the ''dry'' solid line ΔT^{dry}. The solid (dashed) line here corresponds to the solid (dashed) line in Fig. 11(a), i.e., to the linearly n-dependent (n-independent) hydration of the surface-frozen layer. The excellent agreement observed with the measurements for δT_i and ΔT^{wet}, for both n-independent and linearly n-dependent hydration, strongly supports the hydration-difference mechanism suggested here to account for the shifts in the crystallization temperatures and increase in the T ranges of existence.

The discussion above also clarifies the reason for the dramatic decrease observed in the low-n limit for the occurrence of surface freezing. In Fig. 11(b) the ''dry'' ΔT curve becomes negative for $n < 16$, indicating that SF is pre-empted by bulk freezing, so that $T_s < T_f$. Hydration, however, causes an unequal shift in these temperatures, and reverses this relation near the low-n limit. Thus, ΔT becomes positive and surface freezing occurs even for chain lengths as short as $n = 10$. The good agreement between the solid line and the measured ''wet'' ΔT in Fig. 11(b) demonstrates that for this n range the calculations presented above not only predict this lowering of the n limit, but also estimate accurately the measured ΔT ranges. We conclude, therefore, that the increase observed in the n range has the same origin as the increase in ΔT, namely, the unequal upshifts δT_i of the surface and bulk, due to differences in the hydration of the surface between the liquid and crystalline phases.

The high-n limit of the SF effect is not influenced by hydration and remains at $n = 28$ [36], as can be seen in Fig. 11(b). This can be understood by considering the various interactions participating in the SF effect and their variation with chain length and temperature. For n-alkanes, the intermolecular vdW interaction tends to induce order, while the entropy and the formation of gauche kinks at the chain ends tend to reduce the order [6]. A balance of these determines the occurrence or otherwise, and the T and n ranges of the SF effect. In alcohols, the hydroxyl head groups allow for an additional interaction: hydrogen bonding. This, in turn, is responsible for the formation of a bilayer, rather than the monolayer formed in alkanes. This interaction must then be included in the balance that determines the boundaries of existence of SF in alcohols. The hydrogen bonding concerns the headgroup only and is, therefore, chain length *independent* [33]. By contrast, the vdW interaction increases with chain length, as do the entropy (due to the increase in T_f) and the tendency to form gauche conformations at the chain ends (due to the increase in both the melting temperature T_f and chain length). Thus the importance of the hydrogen bond relative to the vdW, entropy, and chain-end disordering decreases quickly with n, and the balance between the ordering and disordering effects at the surface becomes increasingly independent of the hydrogen bonding. Hydration, which affects the hydrogen bonding only, should therefore be most significant for short chains, close to the low-n limit of SF. The large-n limit, on the other hand, is dominated by the balance between intrachain conformational disorder and the interchain vdW interaction. It should thus have a marginal dependence only on changes in the headgroup interactions induced by hydration. These two expectations fully conform to the observations. The reduction in the relative importance of the headgroups' hydrogen bonding is also manifested in the convergence tendency of δT_s toward δT_f, and consequently also of ΔT^{wet} toward ΔT^{dry}, with increasing n, observed in Figs. 11(a) and 11(b). In fact, the figure indicates that if the SF effect was to continue beyond $n = 28$, it would have soon reached the limit of $\delta T_s \approx \delta T_f$, and thus cause the hydration-induced increase in ΔT to vanish. All these effect support the interpretation of a fast decrease of the importance of hydrogen bonding with n in the surface layer, from near dominance at $n \approx 10$ to near insignificance at $n \approx 28$.

To obtain a (very) rough numerical estimate of the binding energies discussed above, we can assume safely that all the disordering interactions (entropy, chain-end disorder) just balance the ordering ones (vdW and hydrogen bonding) at the lower-n limit of SF in dry alcohols. Hydration reduces the low-n limit by ~ 6 carbons, and since the binding energy per CH_2 unit is [43] $\lesssim 1$ kJ mol^{-1}, this represents a ~ 5 kJ mol^{-1} *decrease* in the binding energy. The fact that we still have SF for $n = 10$ means that there must be a corresponding *increase* of ~ 5 kJ mol^{-1} in the only interaction

changed by hydration: hydrogen bonding. Note, however, that this increase is just an upper limit, since by going from $n=16$ (the dry low-n limit) to $n=10$ (the wet low-n limit) we lower also the disordering interactions: we reduce (a) T_f, and thus also the entropic disordering effects, and also (b) the tendency to form gauche kinks at the chain ends, both because of the shorter chain and the lower temperature. It is therefore not unreasonable to assume that the actual increase in hydrogen bonding upon hydration, which balances the reduction in the vdW interaction against the entropic and chain-end disordering effects, is lower, just about 1–2 $\mathrm{kJ\,mol^{-1}}$, in good agreement with the estimate obtained at the beginning of this section from the shift of the $\Delta S_s^{\mathrm{wet}}$ line from the $\Delta S_s^{\mathrm{dry}}$ one in Fig. 6. For the dry alcohol at the high-n limit, the addition of two CH_2 units, with a gain of ~ 2 $\mathrm{kJ\,mol^{-1}}$, is insufficient to compensate for the increase in entropy and the chain-end disordering caused by the increase in T_f and chain length, upon going from $n=28$ to 30, and hence the SF effect vanishes for $n=30$. Apparently, the additional 1–2 $\mathrm{kJ\,mol^{-1}}$ contributed by hydration is still too small to shift the upper limit from $n=28$ to 30. This is hardly surprising, considering that this contribution is equal to, or even smaller than the vdW gain upon addition of two CH_2 units, and is indeed only a small addition to the total binding energy stabilizing the bilayer at the high-n limit, where the vdW interaction alone is of order ~ 30 $\mathrm{kJ\,mol^{-1}}$.

IV. CONCLUSION

We presented an x-ray and surface tension study of dry and hydrated alcohol melts close to, but above, bulk melting. The structure of the bilayer formed was fully characterized in both cases by surface-specific x-ray techniques, and the thermodynamics by surface tension measurements. The water was found to intercalate the surface-frozen bilayer at a water:alcohol molecular ratio of 1:2, and swell the bilayer by about 2.5 Å. The surprising stabilizing influence of hydration on the surface layer was shown to result from differences in hydration between the surface and the bulk in their liquid phase, in accordance to a modified form of the Gibbs adsorption rule, relevant to our case.

It is expected that intercalation of the bilayer by other suitable molecules, able to form hydrogen bonds with the hydroxyl head groups of the alcohols, will allow for varying the structure and properties of the surface-frozen alcohol bilayer in a controlled way. Measurements, now in progress, employing α,ω-diols indicate that this is indeed a viable possibility for molecular-level structural ''engineering'' in these films.

ACKNOWLEDGMENTS

We thank S. K. Sinha (ANL) for important suggestions and discussions, and gratefully acknowledge the support by the Israel Science Foundation, Jerusalem (M.D.), the State of Illinois under HECA (X.Z.W.), and the Petroleum Research Fund administered by the American Chemical Society (X.Z.W.). Brookhaven National Laboratory is supported by the Division of Materials Research, DOE under contract DE-AC02-98CH10886.

[1] J. C. Earnshaw and C. J. Hughes, Phys. Rev. A **46**, R4494 (1992); C. J. Hughes and J. C. Earnshaw, *ibid.* **47**, 3485 (1993).
[2] X. Z. Wu, E. B. Sirota, S. K. Sinha, B. M. Ocko, and M. Deutsch, Phys. Rev. Lett. **70**, 958 (1993).
[3] X. Z. Wu, B. M. Ocko, E. B. Sirota, S. K. Sinha, M. Deutsch, B. H. Cao, and M. W. Kim, Science **261**, 1018 (1993).
[4] E. B. Sirota, H. E. King, Jr., D. M. Singer, and H. H. Shao, J. Chem. Phys. **98**, 5809 (1993).
[5] M. Small, *The Physical Chemistry of Lipids* (Plenum, New York, 1986).
[6] B. M. Ocko, X. Z. Wu, E. B. Sirota, S. K. Sinha, O. Gang, and M. Deutsch, Phys. Rev. E **55**, 3164 (1997).
[7] A. V. Tkachenko and Y. Rabin, Phys. Rev. Lett. **76**, 2527 (1996).
[8] A. V. Tkachenko and Y. Rabin, Phys. Rev. E **55**, 778 (1997).
[9] E. B. Sirota, X. Z. Wu, B. M. Ocko, and M. Deutsch, Phys. Rev. Lett. **79**, 531 (1997); A. V. Tkachenko and Y. Rabin, *ibid.* **79**, 532 (1997).
[10] F. A. M. Leermakers and M. A. Cohen-Stuart, Phys. Rev. Lett. **76**, 82 (1996).
[11] M. Kawamata and T. Yamamoto, J. Phys. Soc. Jpn. **66**, 2350 (1997).
[12] A. Renault, C. Alonso, F. Artzner, B. Berge, M. Goldmann, and C. Zakri, Eur. Phys. J. B **1**, 189 (1998).
[13] G. L. Gaines, *Insoluble Monolayers at the Liquid Gas Interface* (Wiley, New York, 1966).
[14] M. Deutsch, X. Z. Wu, E. B. Sirota, S. K. Sinha, B. M. Ocko, and O. M. Magnussen, Europhys. Lett. **30**, 283 (1995).
[15] M. Deutsch and B. M. Ocko, in *Encyclopedia of Applied Physics*, edited by G. L. Trigg (Wiley, New York, 1998), Vol. 23; J. Als-Nielsen and K. Kjær, in *Phase Transitions in Soft Condensed Matter*, edited by T. Riste and D. Sherrington (Plenum, New York, 1989), p. 245; M. L. Schlossman and P. S. Pershan, in *Light Scattering by Liquid Surfaces and Complementary Techniques*, edited by D. Langevin (Dekker, New York, 1990), p. 365.
[16] A. Braslau, P. S. Pershan, G. Swislow, B. M. Ocko, and J. Als-Nielsen, Phys. Rev. A **38**, 2457 (1988); M. K. Sanyal, S. K. Sinha, K. G. Huang, and B. M. Ocko, Phys. Rev. Lett. **66**, 628 (1991). B. M. Ocko, X. Z. Wu, E. B. Sirota, S. K. Sinha, and M. Deutsch, *ibid.* **72**, 242 (1994).
[17] E. B. Sirota and X. Z. Wu, J. Chem. Phys. **105**, 7763 (1996).
[18] T. Yamamoto, K. Nozaki, and T. Hara, J. Chem. Phys. **92**, 631 (1990).
[19] P. G. deGennes, Rev. Mod. Phys. **57**, 827 (1985).
[20] A. Craievich, I. Denicolo, and J. Doucet, Phys. Rev. B **30**, 4782 (1984).
[21] M. L. Schlossman, D. K. Schwartz, P. S. Pershan, E. H. Kawamoto, G. J. Kellogg, and S. Lee, Phys. Rev. Lett. **66**, 1599 (1991).

[22] J. Majewski, R. Popovitz-Biro, W. G. Bouwman, K. Kjær, J. Als-Nielsen, M. Lahav, and L. Leiserowitz, Chem. Eur. J. **1**, 304 (1995).
[23] G. Vineyard, Phys. Rev. B **26**, 4146 (1982).
[24] D. K. Schwartz, M. L. Schlossman, and P. S. Pershan, J. Chem. Phys. **96**, 2356 (1991); P. S. Pershan, *Structure of Liquid Crystal Phases* (World Scientific, Singapore, 1988); V. M. Kaganer and E. B. Loginov, Phys. Rev. E **51**, 2237 (1995); V. M. Kaganer, I. R. Peterson, R. M. Kenn, M. C. Shih, M. Durbin, and P. Dutta, J. Chem. Phys. **102**, 9412 (1995).
[25] J. Als-Nielsen, D. Jacquemain, K. Kjaer, F. Leveiller, M. Lahav, and L. Leiserowitz, Phys. Rep. **246**, 251 (1994); R. H. Tregold, *Order in Thin Organic Films* (Cambridge University Press, Cambridge, 1994).
[26] The distortion order parameter as measured perpendicular to the chain axis was originally defined as $D=1-(b/a)$ where a and b are the major and minor axes of an ellipse drawn through the six nearest neighbors of a molecule [4]. In I, we denoted this distortion parameter by δ (see Sec. II C in I). Kaganer *et al.* [44] suggested a slight modification, defining the distortion as $\xi=(a^2-b^2)/(a^2+b^2)$. ξ is related to D (or δ) through $\xi=D(1-D/2)/(1-D+D^2/2)$, and they are nearly the same for small distortions. Thus $D=\xi=0$ in the R_{II} rotator phase in alkanes and alcohols, while in the bulk orthorhombic herringbone crystal phase of alcohols the distortion is essentially constant at $D=0.133$ and $\xi=0.142$. For the sake of consistency with the literature [9,44], here we use ξ rather than D.
[27] X. Z. Wu, B. M. Ocko, H. Tang, E. B. Sirota, S. K. Sinha, and M. Deutsch, Phys. Rev. Lett. **75**, 1332 (1995).
[28] E. B. Sirota, Langmuir **13**, 3849 (1997).
[29] B. Berge, L. Fancheux, K. Schwab, and A. Libchaber, Nature (London) **350**, 322 (1991).
[30] C. A. Croxton, *Statistical Mechanics of the Liquid Surface* (Wiley, New York, 1980), Chap. 1.4.
[31] J. Timmermans, *Physico-Chemical Constants of Pure Organic Compounds* (American Elsevier, New York, 1965); C. I. Poser and I. C. Sanchez, J. Colloid Interface Sci. **69**, 539 (1979).
[32] B. Berge, O. Konovalov, J. Lajzerowicz, A. Renault, J.-P. Rieu, M. Vallade, J. Als-Nielsen, G. Grübel, and J.-F. Legrand, Phys. Rev. Lett. **73**, 1652 (1994).
[33] J. P. Rieu and M. Vallade, J. Chem. Phys. **104**, 7729 (1996).
[34] J. L. Wang, F. Leveiller, D. Jacquemain, K. Kjær, J. Als-Nielsen, M. Lahav, and L. Leiserowitz, J. Am. Chem. Soc. **116**, 1192 (1994).
[35] J. Gao and W. L. Jorgensen, J. Phys. Chem. **92**, 5813 (1988).
[36] Measurements on $C_{30}OH$ demonstrate that surface freezing does not occur in this alcohol. Since no samples with $n=32,34,\ldots$, could be obtained for ascertaining the absence of the effect there as well, $n=28$ was assumed to be the upper limit of the n range of existance of surface freezing in alcohols.
[37] O. Gang, B. M. Ocko, X. Z. Wu, E. B. Sirota, and M. Deutsch, Phys. Rev. Lett. **80**, 1264 (1998).
[38] O. Gang *et al.* (unpublished).
[39] A. Doerr, X. Z. Wu, B. M. Ocko, E. B. Sirota, O. Gang, and M. Deutsch, Colloids Surf., A **128**, 63 (1997).
[40] R. Defay and I. Prigogine, *Surface Tension and Adsorption* (Longmans, London, 1966), Chap. XIII; D. G. LeGrand and G. L. Gaines, Jr., J. Polym. Sci., Part C: Polym. Lett. **34**, 45 (1971).
[41] A. S. C. Lawrence *et al.*, J. Phys. Chem. **68**, 3470 (1964); Trans. Faraday Soc. **63**, 2789 (1967); A. S. C. Lawrence and M. P. McDonald, Mol. Cryst. **1**, 205 (1966).
[42] I. Prigogine and J. Marechal, J. Colloid Sci. **7**, 122 (1952).
[43] A. K. Rappe *et al.*, J. Am. Chem. Soc. **114**, 10 024 (1992); S. L. Mayo, B. D. Olafson, and W. A. Goddard III, J. Phys. Chem. **94**, 8897 (1990).
[44] V. M. Kaganer, I. R. Peterson, R. M. Kenn, M. C. Shih, M. Durbin, and P. Dutta, J. Chem. Phys. **102**, 9412 (1995).